

# Adaptive Hybrid Caching for Efficient Text-to-Video Diffusion Model Acceleration

Yuanxin Wei  
Sun Yat-sen University  
Guangzhou, China

Landsong Diao  
Alibaba Group  
Beijing, China

Bujiao Chen  
Alibaba Group  
Beijing, China

Shenggan Cheng  
National University of Singapore  
Singapore

Zhengping Qian  
Alibaba Group  
Beijing, China

Wenyuan Yu  
Alibaba Group  
Beijing, China

Nong Xiao  
Sun Yat-sen University  
Guangzhou, China

Jiangsu Du  
Sun Yat-sen University  
Guangzhou, China

## Abstract

Efficient video generation models are increasingly vital for multimedia synthetic content generation. Leveraging the Transformer architecture and the diffusion process, video DiT models have emerged as a dominant approach for high-quality video generation. However, their multi-step iterative denoising process incurs high computational cost and inference latency, which limits their practical deployment in large-scale and interactive multimedia applications. Caching, a widely adopted optimization method in DiT models, leverages the redundancy in the diffusion process to skip computations in different granularities (e.g., step, cfg, block). Nevertheless, existing caching methods are limited to single-granularity strategies, struggling to balance generation quality and inference speed in a flexible manner. In this work, we propose MixCache, a training-free caching-based framework for efficient video DiT inference. MixCache first distinguishes the interference and boundary between different caching strategies, and then introduces a context-aware cache triggering strategy to determine when caching should be enabled, along with an adaptive hybrid cache decision strategy for dynamically selecting the optimal caching granularity. Extensive experiments on diverse models demonstrate that MixCache can significantly accelerate video generation (e.g., 1.94× speedup on Wan 14B, 1.97× speedup on HunyuanVideo) while delivering both superior generation quality and inference efficiency compared to baseline methods.

## ACM Reference Format:

Yuanxin Wei, Landsong Diao, Bujiao Chen, Shenggan Cheng, Zhengping Qian, Wenyuan Yu, Nong Xiao, and Jiangsu Du. 2026. Adaptive Hybrid Caching for Efficient Text-to-Video Diffusion Model Acceleration. In . ACM, New York, NY, USA, 11 pages. <https://doi.org/10.1145/nnnnnnn.nnnnnnn>

Permission to make digital or hard copies of all or part of this work for personal or classroom use is granted without fee provided that copies are not made or distributed for profit or commercial advantage and that copies bear this notice and the full citation on the first page. Copyrights for components of this work owned by others than the author(s) must be honored. Abstracting with credit is permitted. To copy otherwise, or republish, to post on servers or to redistribute to lists, requires prior specific permission and/or a fee. Request permissions from [permissions@acm.org](mailto:permissions@acm.org).  
*Conference'17, Washington, DC, USA*

© 2026 Copyright held by the owner/author(s). Publication rights licensed to ACM.  
ACM ISBN 978-x-xxxx-xxxx-x/YYYY/MM  
<https://doi.org/10.1145/nnnnnnn.nnnnnnn>

## 1 Introduction

Diffusion Transformer (DiT) [25] has revolutionized video generation by integrating the scalability of the Transformer architecture [31] with the power of the diffusion process [6, 26], enabling unprecedented quality in synthetic video creation. Recent advances in video DiT models, such as SD3.0 [5], Sora [2], CogVideoX [38], and Wan [32], have greatly expanded the capabilities of multimedia systems, supporting a wide range of applications including text-to-video generation [11, 36], video editing [9, 33], and video continuation [38]. Such advancements not only improve the fidelity and variety of generated multimedia content but also open new possibilities for creative expression in video-based applications.

Despite achieving superior fidelity, the inference of video DiT models relies on an iterative denoising process, which demands substantial computation and hinders time-sensitive deployment. Starting from a random Gaussian noise initialization, these models require tens of denoising steps, typically ranging from 20 to 100, to progressively reconstruct high-quality video. Consequently, generating a 5-second 720p video with a single GPU can take 50 minutes, presenting a significant latency bottleneck.

The research community has made significant efforts to speed up video DiT models. Among them, caching-based acceleration has emerged as one of the most widely adopted approaches. Caching can reduce redundant computation and improve efficiency by storing and reusing intermediate features, leveraging output similarity across diffusion timesteps. According to the caching granularity from coarse to fine, existing caching methods can be divided into step level [10, 15, 23], cfg level [20], block level [13, 21, 22, 28, 29, 35, 43], and token level [16, 44, 45].

However, existing caching methods primarily exploit output redundancy at a single granularity, overlooking the inherent redundancy across multiple granularities throughout the diffusion process. This narrow focus compromises the balance between generation quality and computational efficiency. Through systematic investigation, we demonstrate that adaptively combining caching methods at diverse granularities enables more effective utilization of output redundancy. In this paper, we propose MixCache, a training-free, caching-based inference framework for video DiT models that enables flexible integration of caching methods with varying granularities. This hybrid caching framework provides more effective

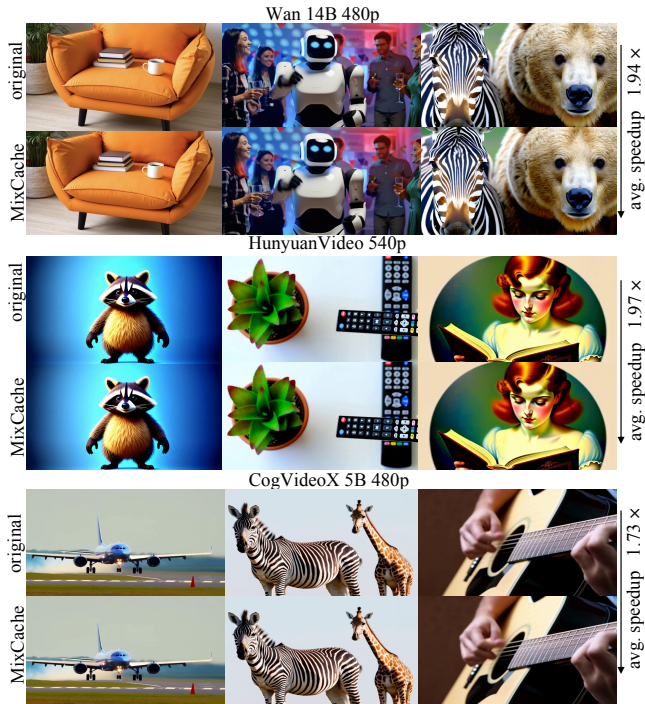


Figure 1: MixCache visualization across video DiT models.

acceleration for video DiT inference while preserving generation quality.

Our contributions are as follows:

- We conduct a comprehensive analysis of redundancy across multiple granularities in the diffusion process, including step level, cfg level and block level, and reveal the dynamism nature of redundancy.
- We propose a context-aware cache triggering strategy to determine when to enable caching, along with an adaptive hybrid cache decision strategy to determine the caching granularity (step/cfg/block) in a flexible manner for each timestep.
- Building upon the above strategies, we present MixCache, a training-free caching-based inference framework that adaptively integrates multi-granularity caching methods without modifications to model structure.
- Extensive experiments on industrial-scale video DiT models show that MixCache demonstrates significant improvement in inference speed while maintaining high video quality.

## 2 Related Works

In the following, we introduce works that are highly related to our method.

**Step level caching.** Recent DiT advancements introduce diverse step level caching strategies. TeaCache [15] leverages input-output correlations by estimating timestep embeddings to implement a dynamic caching. AdaCache [10] dynamically evaluates step-wise differences to determine skip lengths. AB Cache [39] extends prior methods by reusing combined outputs from the previous  $k$  steps,

rather than a single-step result. NIRVANA [1] diverges from these intra-generation approaches by enabling cross-generation cache reuse to skip computation of preceding sampling timesteps.

**CFG level caching.** Recent studies leverage cfg similarities to accelerate diffusion inference. FasterCache [20] exploits the similarity between conditional and unconditional outputs at the same timestep to construct a cfg level cache mechanism. DiTFastAttn [40] identifies consistent attention patterns in specific attention heads of conditional and unconditional inference, implementing cfg level attention sharing to bypass redundant computation.

**Block level caching.** For the DiT architecture, recent works propose block level caching with varying strategies. FORA [28], PAB [43], and BlockDance [41] employ static interval-based block skipping (e.g., MLP/attention blocks).  $\Delta$ -DiT [3] adopts a phase-specific caching strategy, storing back blocks during early stages and front blocks in later stages. L2C [21] and MD-DiT [29] implement dynamic runtime caching through learnable layer selection and gradient-free search mechanisms, respectively.

**Other optimizations.** Recent works [14, 16, 44, 45] have explored token redundancy (such as background areas) to reduce computational cost. However, the dynamic nature and dataset-dependent characteristics of input tokens necessitate extensive code modifications to transformer blocks for implementation, resulting in poor compatibility. Moreover, the acceleration efficiency of token level caching is fundamentally limited by its fine-grained caching granularity and the overhead of token importance scoring. In response to the performance bottleneck caused by the multi-step iterative characteristic of the diffusion process, some works also explore efficient solvers, including DDIM [30], DPM-Solver [17] and DPM-Solver++ [18]. Additionally, distillation-based methods [19, 24, 27] have been developed to compress the number of diffusion sampling timesteps.

## 3 Methodology

### 3.1 Preliminary

**Diffusion model** is a generative model consisting of a forward process and a reverse process. In the forward diffusion process, given an original video  $x_0$  and a random timestep  $t$ , the video after  $t$  diffusion timesteps is:

$$x_t = \sqrt{\delta_t}x_{t-1} + \sqrt{1 - \delta_t}\epsilon_t, \quad t = 1, 2, \dots, T \quad (1)$$

where  $\delta_t$  is a schedule coefficient that varies with  $t$ , and  $T$  is the total sampling timesteps. A noise estimation network plays a critical role in approximating the noise distribution in the diffusion process. Specifically, it aims to minimize the discrepancy between the predicted noise term  $\epsilon_\theta$  and the actual noise  $\epsilon$ . In most current works, the noise estimation network adopts the DiT architecture, where the predicted noise function  $\epsilon_\theta(x_t)$  can be further reformulated as:

$$\begin{aligned} \epsilon_\theta(x_t) &= f_{L-1}(f_{L-2}(\dots(f_0(x_t)))) \\ &= f_{L-1} \circ f_{L-2} \circ \dots \circ f_0(x_t) \end{aligned} \quad (2)$$

where  $f_n$  represents the  $n$ -th DiT block and  $L$  represents the total number of DiT blocks.

The inference process, defined as the reverse transformation of noisy data into clean output, is a crucial part of the diffusion process. Initially, a random Gaussian noise  $X_T$  is given. It is input

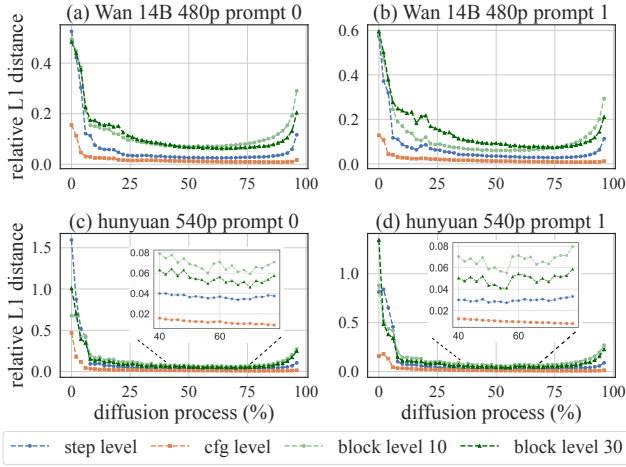


**Figure 2: Three levels of redundancy across denoising timesteps in Wan 14B 480p and HunyuanVideo 540p.**

into the noise estimation network  $\epsilon_\theta$  to obtain the noise estimate  $\epsilon_\theta(x_T)$ . According to specific sampling solver  $\Phi$ , the noisy video is denoised to produce the denoised sample  $x_{T-1}$  after one timestep. After iterating this process  $T$  times, the final generated video is obtain.

$$x_{t-1} = \Phi(x_t, t, \epsilon_\theta(x_t)), \quad t = T, T-1, \dots, 1 \quad (3)$$

**Classifier-Free Guidance (CFG)** has proven to be a powerful technique for improving the fidelity of generated videos in diffusion models. During the sampling process, CFG generates two distinct predictions: the conditional output  $\epsilon_\theta(x_t, t, c)$  conditioned on the input context  $c$ , and the unconditional output  $\epsilon_\theta(x_t, t, \phi)$  derived from the empty/negative prompt  $\phi$ . The final denoised output is:

$$\tilde{\epsilon}_\theta(x_t, t, c) = (1 + g) \cdot \epsilon_\theta(x_t, t, c) - g \cdot \epsilon_\theta(x_t, t, \phi) \quad (4)$$

where  $g$  is the guidance scale. While CFG significantly enhances visual quality, it also increases computational cost and inference latency due to the additional computation required for unconditional outputs.

### 3.2 Analysis and Motivation

**Three levels of redundancy.** There exists three levels of redundancy in the diffusion process. The first type refers to the **step level** redundancy, which manifests as high similarity between consecutive timestep outputs. The second type is the **cfg level** redundancy, indicating that the outputs of conditional forward and unconditional forward within the same timestep are similar. The third type is **block level** redundancy, which means that the output of some transformer blocks at this timestep is similar to the output of the same block at the previous timestep. We adopt the relative L1 distance to characterize the similarity of two outputs, and the

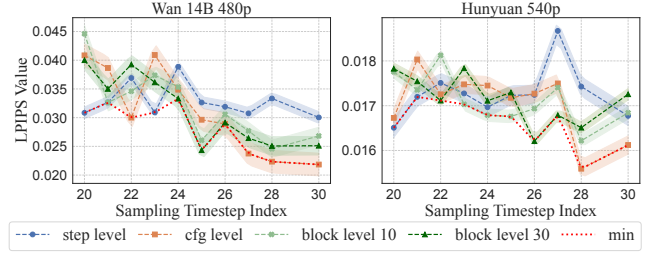


**Figure 3: Similarity metric compared with the original model using different cache strategies in different timesteps.**

three-level redundancy is measured as follows:

$$D_t^{step} = \frac{\|O_t^{step} - O_{t-1}^{step}\|_1}{\|O_{t-1}^{step}\|_1}$$

$$D_t^{cfg} = \frac{\|O_t^{uncond} - O_t^{cond}\|_1}{\|O_t^{cond}\|_1} \quad (5)$$

$$D_t^{block_i} = \frac{\|O_t^{block_i} - O_{t-1}^{block_i}\|_1}{\|O_{t-1}^{block_i}\|_1}, \quad i \in [0, L]$$

where  $t$  denotes the sampling timestep index, advancing incrementally as the diffusion process progresses. The smaller the  $D$  value, the higher the similarity between two outputs. As presented in Figure 2, we use different prompts to examine the different-level redundancy on Wan and HunyuanVideo. Such redundancy offers opportunities for caching-based computation skipping to enhance inference efficiency.

**The dynamism of redundancy.** In Figure 2, the redundancy during the diffusion process shows strong dynamism. Specifically, there are the following manifestations: (1) All of the three-level redundancy demonstrates strong correlations across timesteps: the initial distance value is relatively high, and gradually decreases and stabilizes. This indicates that the early diffusion stage is sensitive with low redundancy, thereby making it unsuitable for caching. (2) The speed at which redundancy decreases varies among different prompts. (3) The degree of redundancy varies with different levels. For example, in Wan, the cfg level redundancy always remains the strongest throughout the diffusion process. The redundancy of block 10 in the early diffusion stage is stronger than that of block 30, while it is weaker than block 30 in the later diffusion stage. The above phenomenons necessitate an adaptive and unified hybrid caching mechanism.

**Potential of three-level cache integration.** We implement different granularity caching methods at each diffusion timestep, and adopt the LPIPS [42] metric to calculate the end-to-end similarity with the original video. The smaller the LPIPS value, the higher the similarity. As shown in Figure 3, the optimal cache granularity varies dynamically across timesteps, suggesting that adaptive cache selection could enhance generation quality.

In order to better integrate different caching granularities, there are two core issues: (1) When will caching be triggered? That is, which timesteps enable caching and which perform full computation? (2) Which caching granularity should be selected for a given cache enabled timestep? To address the above issues, we propose

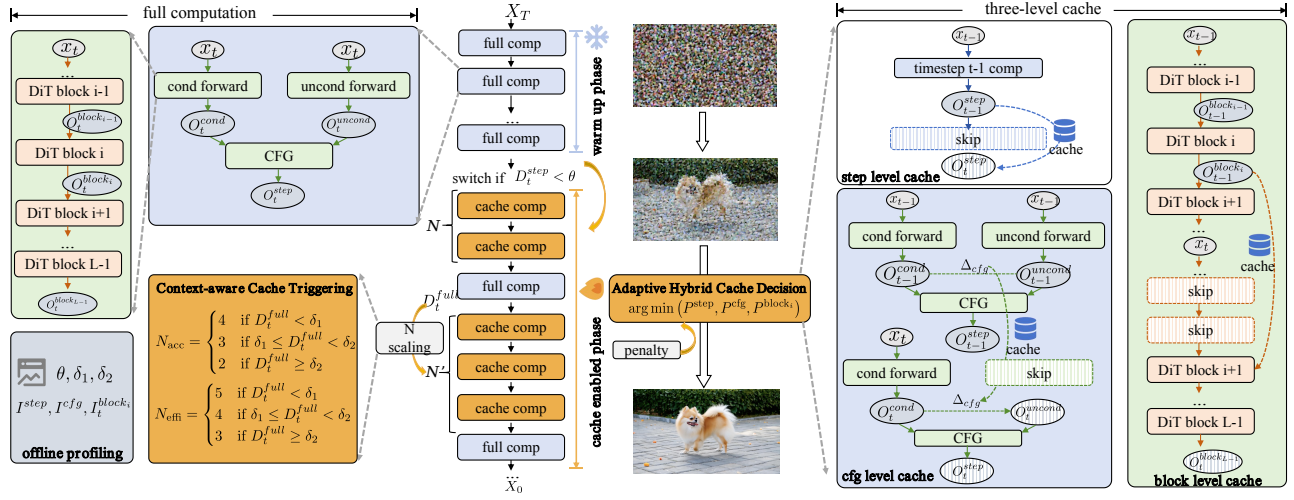


Figure 4: The MixCache framework.

the context-aware cache triggering strategy and adaptive hybrid cache decision strategy, respectively. Integrating these two strategies, we propose the MixCache framework, aiming to achieve video DiT inference acceleration while maintaining a comparable quality of video generation. The overall MixCache framework is demonstrated in Figure 4.

### 3.3 Context-aware Cache Triggering

As the early diffusion stage is responsible for overall framework sketching, it is highly sensitive to interference at this time, as described in SRDiffusion [4]. This phenomenon can also be validated in Figure 2, where in the initial diffusion process, the three-level redundancy is relatively low. Therefore, we perform full computation in the initial diffusion stage, and calculate  $D_t^{step}$  between the output of the current timestep  $t$  and that of the previous timestep  $t - 1$ , and we call this stage as the *warm up stage*. When  $D_t^{step}$  is smaller than the predefined threshold  $\theta$ , established in the offline profiling process (detailed later), the warm up phase ends and enters the *cache enabled phase*.

Once entering the cache enabled phase, in order to ensure the quality of video generation, it is necessary to perform full computation at certain intervals. A key issue is to determine which timesteps to perform full computation, and we refer to the number of cache enabled steps between two full computation timesteps as *cache interval* (represented as  $N$  in Figure 4). In Figure 2, we observed that, after the warm up phase, the step level redundancy stabilizes at a certain value. Based on this, we propose an adaptive  $N$  scaling strategy designed to dynamically monitor the deviation magnitude between the cached output and the ground-truth output, and automatically adjust the cache interval to maintain generation quality. Specifically, after entering the cache enabled phase, we compare the output of two consecutive full computation, namely  $D_t^{full}$ , measured in relative L1 distance. When  $D_t^{full}$  exceeds threshold  $\delta_2$ , this indicates the current cache granularity is too aggressive, requiring a reduction in the subsequent cache interval. Conversely,

if it falls below  $\delta_1$ , the next cache interval should be increased. In order to balance quality and efficiency, we provide two cache interval configurations, namely 2/3/4 ( $N_{acc}$ ) and 3/4/5 ( $N_{eff}$ ), which prioritize accuracy and efficiency respectively. The accuracy-prior cache interval  $N_{acc}$  has a higher full computation frequency, resulting in better video generation quality:

$$N_{acc} = \begin{cases} 4 & \text{if } D_t^{full} < \delta_1 \\ 3 & \text{if } \delta_1 \leq D_t^{full} < \delta_2 \\ 2 & \text{if } D_t^{full} \geq \delta_2 \end{cases} \quad (6)$$

### 3.4 Adaptive Hybrid Cache Decision

After identifying cache enabled timesteps, it is crucial to determine the specific caching granularity for a certain timestep within the three-level caching. The limitation of prior works [14, 15, 23] is their exclusive focus on similarity of different cache methods while neglecting their differential impact on accuracy. To assess the accuracy impact of different caching methods, we generate Gaussian distribution with predefined statistical parameters (mean  $\hat{\mu}$ , standard deviation  $\hat{\sigma}$ ) and calculate the distance between perturbed and original outputs. It should be noted that  $\hat{\mu}$  and  $\hat{\sigma}$  should align with the real parameters derived from the three-level caching. Therefore, we firstly profile prompts and examine the  $\mu$  and  $\sigma$  of the distance tensor between the real output and the cached output. As shown in Figure 6, the  $\mu$  value of the distance tensor is inconsistent across different prompts, and also varies at different timesteps. However, its values are fixed within a certain range. Therefore, we set the  $\hat{\mu}$  value as the average of  $\mu$  value across all timesteps. In addition, for the  $\hat{\sigma}$  value, except for the initial timesteps, it remains stable at a fix value. Therefore, we set the  $\hat{\sigma}$  value as the average of the  $\sigma$  value of the last 40 timesteps. We exclude the first 10 timesteps from analysis since these initial timesteps correspond to the warm up phase without applying caching. Consequently, their outputs lack statistical representativeness for evaluating the proposed methodology.

After determining the  $\hat{\mu}$  and  $\hat{\sigma}$  value, we examine the relative L1 distance between the perturbed output and the original output.

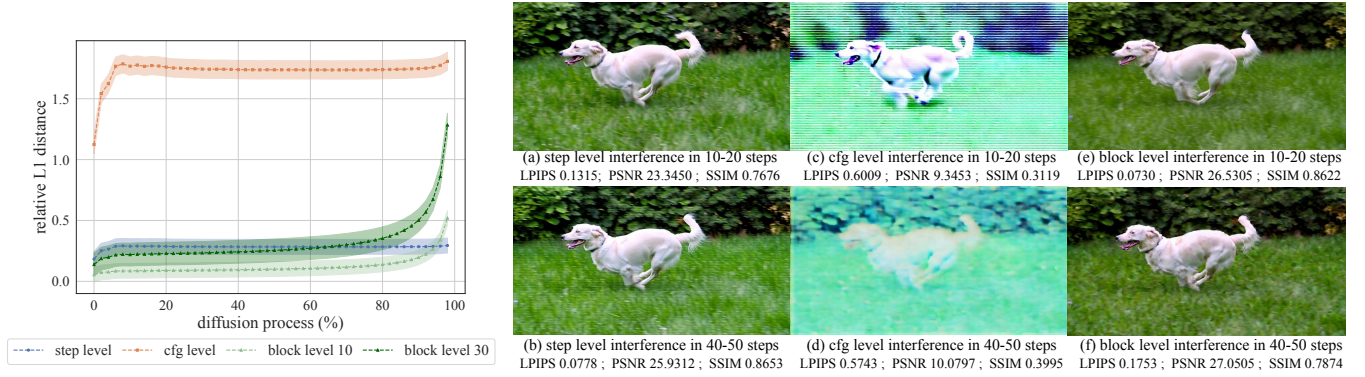


**Figure 5: (a) left: Distance between the perturbed and original output, which performs as the impact indicator. (b) right: Visualization and quantitative metrics (LPIPS ↓ PSNR ↑ SSIM ↑) of different level interference at different diffusion stages.**

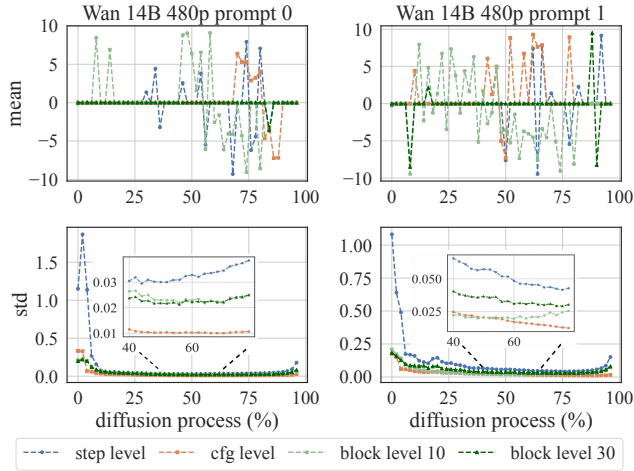


**Figure 6: The value of mean  $\mu$  and standard deviation  $\sigma$  of the distance tensor between the cached output and the original output.**

We examine for all timesteps and plot the results in Figure 5(a). The smaller the distance, the smaller the impact of the interference on the actual results. This value can indicate the accuracy impact of performing a specific level cache at a specific timestep. From Figure 5(a), it can be seen that the impact value of step level and cfg level remain relatively stable after the warm up phase. However, the block level value exhibits time-dependent characteristics, where its initial value is low, and then increases in the later diffusion stage. In addition, the compare across three levels reveals that, the cfg level interference exerts a substantially greater influence, with its value exceeding both step level and block level interference by an order of magnitude. We present the visualized results and similarity metrics in Figure 5(b). It can be seen that the video quality generated using cfg level interference is poor, indicating that this interference has a significant impact on the final results, which is consistent with the conclusion in Figure 5(a). Therefore, the values presented in Figure 5(a) are employed as quantitative evaluation metrics for assessing accuracy impact, with the impact of step level and cfg level remaining constant ( $I^{step}$ ,  $I^{cfg}$ ), while the block level impact

exhibit as a time-dependent and index-dependent function ( $I_t^{block_i}$ ). Thus, the offline Gaussian perturbation estimates the quantified impact value for each cache type using  $\hat{\mu}$  and  $\hat{\sigma}$  fit from measured cache-induced differences.

The similarity and accuracy impact jointly determine the final generated video quality. We prefer to employ the caching method with a lower similarity and a lower impact, as it indicates that such method exerts minimal influence on the generated video. Therefore, we utilize the product of these two values to represent the final metric, measured as  $P$  value. After each cache enabled timestep, we calculate the similarity of the three levels and get  $D_t^{step}$ ,  $D_t^{cfg}$ ,  $D_t^{block_i}$ , and product them with the corresponding impact value. Based on the greedy principle, we choose the cache method with the smallest  $P$  as the cache method of the next cache enabled timestep.

$$P_t^\psi = D_t^\psi \cdot I_t^\psi, \psi \in \{step, cfg, block_i\} \quad (7)$$

where  $i$  is one of the pre-defined block indices. To prevent getting stuck in the same caching granularity within a cache interval, we introduce a *penalty strategy*: if a caching granularity is used in one timestep, it is disabled in the next timestep. This proactive approach ensures flexibility and robustness, enabling systems to avoid local optima.

### 3.5 Unify it together: MixCache Framework

The context-aware cache triggering strategy and adaptive hybrid cache decision strategy solve the issue of when to enable caching and which cache granularity to select, respectively. Unifying these two strategies, we obtain the MixCache framework. MixCache provides a training-free and adaptive hybrid cache mechanism that can effectively combine three three-level caching, achieving a balance between generation quality and inference speed.

According to Figure 2, the redundancy level of different models varies. Given a specific model, MixCache first performs offline profiling to determine key hyper-parameters. We run 100 prompts through the diffusion process, recording  $D^{step}$  at each timestep. Once  $D^{step}$  stabilizes, which is identified when its value remains below a certain value compared to the previous five steps, we compute the average as  $\theta$ . The maximum and minimum deviations from  $\theta$  after stabilization are set as  $\delta_1$  and  $\delta_2$ . These values are averaged

**Algorithm 1** The execution flow of the MixCache framework

---

```

1: Offline Profiling: Obtain  $\theta, \delta_1, \delta_2, I^{\text{step}}, I^{\text{cfg}}, I_t^{\text{block}_i}$ 
2: Initialize: cache interval  $N$ ,  $\text{cnt} = 0$ 
3: for each sampling timestep  $t \in \{0, 1, 2, \dots, T - 1\}$  do
4:   Compute  $D_t^{\text{step}}, D_t^{\text{cfg}}, D_t^{\text{block}_i}$ 
5:   if  $D_t^{\text{step}} \geq \theta$  then ▷ Warm-up phase
6:     Perform full computation
7:   else ▷ Cache enabled phase
8:      $\text{cnt} \leftarrow (\text{cnt} + 1) \% N$ 
9:     if  $\text{cnt} == 0$  then
10:       Perform full computation
11:       Compute  $D^{\text{full}}$  and scale  $N$ 
12:     else if cache mode is step level then
13:        $O_t \leftarrow O_{t-1}$ 
14:     else if cache mode is cfg level then
15:        $O_t^{\text{cond}} \leftarrow$  conditional forward output
16:        $O_t^{\text{uncond}} \leftarrow O_t^{\text{cond}} + \Delta_{\text{cfg}}$ 
17:        $O_t \leftarrow \text{CFG}(O_t^{\text{cond}}, O_t^{\text{uncond}})$ 
18:     else if cache mode is block level  $i$  then
19:       Input for block  $i + 1 \leftarrow O_{t-1}^{\text{block}_i}$ 
20:       Execute DiT block[ $i+1$ :]
21:        $O_t^{\text{uncond}} \leftarrow O_t^{\text{cond}} + \Delta_{\text{cfg}}$ 
22:        $O_t \leftarrow \text{CFG}(O_t^{\text{cond}}, O_t^{\text{uncond}})$ 
23:        $P_t^\psi \leftarrow D_t^\psi \cdot I^\psi, \psi \in \{\text{step}, \text{cfg}, \text{block}\}$ 
24:       cache mode  $\leftarrow \arg \min (p^{\text{step}}, p^{\text{cfg}}, p^{\text{block}_i})$ 

```

---

across all prompts and rounded as needed. The profiling also determines  $\hat{\mu}$  and  $\hat{\sigma}$  for Gaussian interference, used to assess impact at different granularities. This process is performed once per model and enables efficient runtime deployment without extra overhead.

After the offline profiling process, it enters the runtime inference phase, and the execution flow is formalized in Algorithm 1. During runtime, one generation is partitioned into two distinct phases: the warm up phase and the cache enabled phase. In the warm up phase, the system exclusively executes full computations to maintain video quality, and this phase is ended by the context-aware cache triggering strategy to determine which timestep to enable caching (line 5). Once into the cache enabled phase, MixCache uses the adaptive hybrid cache decision strategy to determine which of the three-level caching methods to use. There are two core mechanisms are activated: (1) the  $N$  scaling strategy to regulate the frequency of cache interval (line 11), and (2) the adaptive hybrid cache decision strategy (line 23-24) that dynamically determines the optimal caching granularity for each timestep.

## 4 Experiments

### 4.1 Settings

**Base Models and Baselines.** We evaluate MixCache on Wan2.1 14B [32], HunyuanVideo [12] and CogVideoX 5B [38]. For baseline methods, we choose Teacache [15], FasterCache [20], BlockDance [41] and PAB [43], all of which are specifically designed to accelerate DiT models through caching. Among them, Teacache

Methods	Visual Quality				Efficiency	
	Vbench $\uparrow$	LPIPS $\downarrow$	PSNR $\uparrow$	SSIM $\uparrow$	Latency	Speedup
<b>Wan 14B</b> (832 $\times$ 480, 5s, 81 frames, T = 50)						
original	84.05	-	-	-	900 s	-
Teacache <sub>0.1</sub>	<b>84.01</b>	0.147	22.17	0.786	849 s	1.06 $\times$
Teacache <sub>0.14</sub>	83.95	0.244	18.60	0.688	612 s	1.47 $\times$
FasterCache	83.40	0.140	23.26	0.796	633 s	1.42 $\times$
BlockDance <sub>4</sub>	83.48	0.129	<b>24.01</b>	0.811	679 s	1.29 $\times$
PAB <sub>100,800</sub> <sup>8</sup>	83.00	0.166	22.29	0.772	717 s	1.25 $\times$
MixCache <sub>acc</sub>	83.97	<b>0.124</b>	23.45	<b>0.814</b>	528 s	1.70 $\times$
MixCache <sub>effi</sub>	83.90	0.132	22.94	0.804	<b>465 s</b>	<b>1.94<math>\times</math></b>
<b>Wan 14B</b> (1280 $\times$ 720, 5s, 81 frames, T = 50)						
original	83.66	-	-	-	3168 s	-
Teacache <sub>0.1</sub>	83.75	0.148	22.58	0.813	2988 s	1.06 $\times$
Teacache <sub>0.14</sub>	<b>83.78</b>	0.237	19.24	0.732	2155 s	1.47 $\times$
FasterCache	83.12	0.156	22.97	0.806	2230 s	1.42 $\times$
BlockDance <sub>4</sub>	83.43	0.136	23.70	0.820	2455 s	1.29 $\times$
PAB <sub>100,800</sub> <sup>8</sup>	83.32	0.195	21.41	0.775	2534 s	1.25 $\times$
MixCache <sub>acc</sub>	83.74	<b>0.132</b>	<b>23.88</b>	<b>0.824</b>	1951 s	1.62 $\times$
MixCache <sub>effi</sub>	83.70	0.146	22.81	0.815	<b>1742 s</b>	<b>1.82<math>\times</math></b>
<b>HunyuanVideo</b> (960 $\times$ 544, 5s, 129 frames, T = 50)						
original	81.13	-	-	-	2289 s	-
Teacache <sub>0.1</sub>	80.87	0.247	17.57	0.734	1421 s	1.61 $\times$
BlockDance <sub>4</sub>	80.93	0.051	<b>28.80</b>	0.897	1646 s	1.39 $\times$
PAB <sub>100,800</sub> <sup>8</sup>	80.64	0.066	28.56	0.901	1847 s	1.24 $\times$
MixCache <sub>acc</sub>	<b>81.05</b>	<b>0.047</b>	28.37	<b>0.921</b>	1240 s	1.84 $\times$
MixCache <sub>effi</sub>	80.98	0.060	26.86	0.906	<b>1151 s</b>	<b>1.97<math>\times</math></b>
<b>CogVideoX 5B</b> (820 $\times$ 480, 6s, 49 frames, T = 50)						
original	80.89	-	-	-	443 s	-
Teacache <sub>0.1</sub>	<b>80.15</b>	0.239	20.42	0.741	289 s	1.53 $\times$
BlockDance <sub>4</sub>	74.34	0.349	24.76	0.750	348 s	1.27 $\times$
PAB <sub>100,800</sub> <sup>8</sup>	78.67	0.235	21.69	0.770	293 s	1.51 $\times$
MixCache <sub>acc</sub>	80.10	<b>0.089</b>	<b>34.33</b>	<b>0.892</b>	287 s	1.54 $\times$
MixCache <sub>effi</sub>	<b>80.15</b>	0.160	26.86	0.880	<b>256 s</b>	<b>1.73<math>\times</math></b>

Table 1: Comparison of efficiency and visual quality.

adopts step level cache, FasterCache combines cfg level and block level cache, and BlockDance and PAB employ block level cache. We adjust the parameters of each baseline to achieve a balance between speed and quality. Specifically, Teacache<sub>0.1</sub> indicates that the value of L1\_distance\_thresh from the open-source implementation is set to 0.1, and the implementation of PAB is adopted on HuggingFace Diffusers, where PAB<sub>100,800</sub><sup>8</sup> denotes a configuration of block\_skip\_range=8 and timestep\_skip\_range=[100, 800]. For BlockDance<sub>N</sub>, following the official setting, we set the cache block index as 20 and set the first 40% of denoising steps as warm up steps that disable caching, and evenly divide the remaining 60% of denoising steps into several groups, each comprising  $N$  steps.

**Evaluation Metrics.** To evaluate the quality of video generation, we employ VBench [7], a widely-adopted comprehensive benchmarking suite for evaluating video generation. Based on VBench standard prompt set, we use Qwen2.5-14B-Instruct [37] to extend all prompts to enhance the video quality, and generate 5 videos with different seeds for each prompt. In addition, we report LPIPS [42], SSIM [34] and PSNR for quality comparison. For efficiency evaluation, we quantify the average inference latency per prompt as the primary performance metric.



Figure 7: Visual quality comparison. MixCache delivers high quality and maintains consistency with original results.

**Experiment Settings.** For the main results, we generated 4720 videos for each set of results based on VBench. These were processed in data parallel across a public cloud instance with 64 NVIDIA A800 (80GB) GPUs, and the whole experiment takes nearly a month to complete. Except the main results that use all prompts of VBench, we randomly sample 200 prompts from VBench to conduct ablation experiments, each using 1 seed for generation.

**Implementation Details.** All experiments conduct full attention inference. We pre-defined block index as (10,20,30) as block caching candidates, which performs well for most models. The profiled hyper-parameters  $\theta$  and  $(\delta_1, \delta_2)$  for Wan and HunyuanVideo are 0.1, (0.05, 0.1), respectively, and those for CogVideoX are 0.1, (0.3, 0.4) respectively.

## 4.2 Main Results

**Quantitative Comparison.** Table 1 presents a quantitative comparison of MixCache with baselines in terms of efficiency and visual quality. The results highlight that, MixCache consistently demonstrates robust acceleration efficiency and maintains visually compelling quality across diverse base models, baselines, and resolutions.

**Visual Comparison.** Figure 7 compares the videos generated by MixCache against those by the original model and baselines. The results demonstrate that MixCache can effectively preserve the original semantics and fine details.

## 4.3 Ablation Study

In the ablation study, we investigate the effects of  $N$  scaling strategy, penalty strategy and hybrid three-level caching respectively in terms of the quality and efficiency. The quantitative results are shown in Table 2 and the corresponding visualization results are presented in Figure 8. Among them, “hybrid” refers to using the adaptive hybrid cache decision strategy to determine the cache method for each cache enabled step, while “step/cfg/block only” refers to using only a specific caching method in all cache enabled steps. “ $N=4$ ” represents a fixed cache interval of 4, and “ $N_{\text{eff}}$ ” represents enabling the  $N$  scaling strategy that prioritizes efficiency. It



prompt: A sleek modern car driving alongside a fast-moving train on parallel tracks, both moving towards the right side of the frame. Mid-shot, dynamic camera movement following the vehicles.

Figure 8: Visualization of ablation study on Wan 14B 480p.

can be seen that MixCache outperforms all ablation experiments in both quality and efficiency metrics, indicating that combining dynamic  $N$  scaling, penalty strategy and hybrid three-level caching can achieve better generation quality and inference efficiency.

Method	LPIS ↓	PSNR ↑	SSIM ↑	Latency	Speedup
original	-	-	-	900 s	-
hybrid + $N=4$	0.082	25.74	0.854	593 s	1.51 ×
step only + $N_{\text{eff}}$	0.147	22.25	0.775	545 s	1.65 ×
cfg only + $N_{\text{eff}}$	0.080	25.90	0.853	623 s	1.44 ×
block only + $N_{\text{eff}}$	0.114	24.62	0.809	537 s	1.67 ×
MixCache <sub>eff</sub> wo. pen	0.102	23.75	0.796	525 s	1.71 x
MixCache <sub>eff</sub> wi. pen	<b>0.079</b>	<b>25.91</b>	<b>0.858</b>	<b>465 s</b>	<b>1.94 x</b>

Table 2: The ablation study of  $N$  scaling strategy, penalty strategy and three-level caching on Wan 14B 480p.

## 4.4 Adaptability

As shown in Figure 9, we present the distribution of three-level caching across three models, evaluated on two distinct prompts. Through intra-model comparison across different prompts, it is evident that both the number of cache enabled timesteps and the

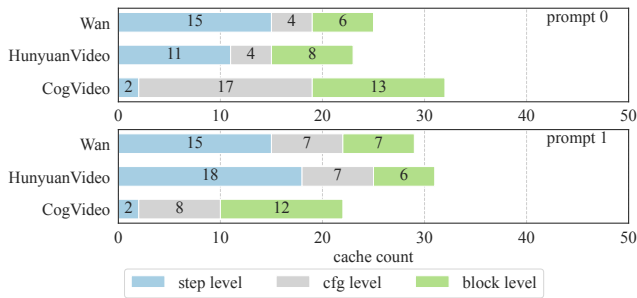


Figure 9: Distribution of three-level caching on two prompts.

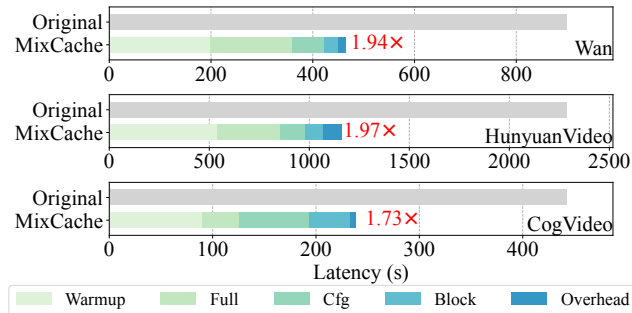


Figure 10: Latency breakdown on three models.

distribution across three levels exhibit significant variations. Inter-model analysis reveals distinct cache utilization patterns. For instance, CogVideoX exhibits relatively fewer step level caching compared to other models, which attributes to its unique architectural property. These observations highlight the inherent adaptability of MixCache in accommodating diverse model architectures and prompts through context-aware resource allocation.

#### 4.5 Latency Breakdown

Figure 10 shows the latency breakdown of MixCache<sub>eff</sub> on three models. Among them, “Full” indicates the time for performing full computations at adaptive intervals after entering the cache enabled phase. “Overhead” is primarily used for determining cache intervals, calculating  $D$  values, and selecting cache modes for each step. As step-level caching skips all the computation of that step, it is not included in the breakdown. As can be seen, MixCache’s performance benefit primarily comes from significantly reducing full computation time with minimal overhead.

#### 4.6 Hyperparameter Selection

We conduct experiments under different hyperparameter configurations on a wan 14B 480p with 200 prompts. Figure 11 plots the generated quality (indicated by PSNR  $\uparrow$ ) and latency for: (a) varying  $\theta$  with  $(\delta_1, \delta_2)=(0.05, 0.1)$  and (b) varying  $(\delta_1, \delta_2)$  with  $\theta=0.1$ . As can be seen, under different configurations, there is a trade-off between quality and latency. Specifically, Figure 11(a) shows that,

Block Candidate	LPIPS $\downarrow$	PSNR $\uparrow$	SSIM $\uparrow$	Latency	Mem.
(20)	0.093	25.04	0.803	483 s	0.64 GB
(10,30)	0.089	25.22	0.821	470 s	1.27 GB
(10,20,30)	<b>0.079</b>	<b>25.91</b>	<b>0.858</b>	<b>465 s</b>	<b>1.89 GB</b>
(10,15,20,25,30,35)	0.080	25.86	0.849	468 s	3.77 GB

Table 3: Quality, latency and memory overhead under different block candidates on Wan 14B 480p.

when fixed  $(\delta_1, \delta_2)=(0.05, 0.1)$ , while  $\theta=0.08$  or  $0.05$  has a slight improvement in generated quality compared to  $\theta=0.1$ , it suffers from a significant disadvantage in latency. This phenomenon can also be seen in Figure 11(b). Therefore, considering the trade-off between quality and speed, we choose the configuration with  $\theta=0.1$  and  $(\delta_1, \delta_2)=(0.05, 0.1)$ .

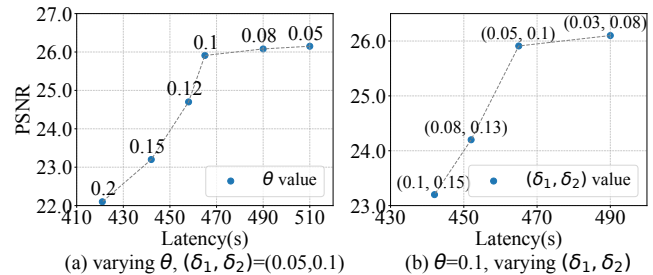


Figure 11: Quality-latency tradeoff under different hyperparameter configurations on Wan 14B 480p.

#### 4.7 Block Candidate Selection

We experiment the effects of different block candidates on quality, latency, and memory overhead. As shown in Table 3, the more block candidates, the more extra memory overhead will be incurred, as more block outputs need to be saved for caching. However, a larger number of block candidates does not necessarily lead to improvements in generation quality and speed. In addition, if there are too few block candidates, the generation quality will drop significantly, since the block level caching cannot capture the different features of different blocks. Therefore, we select (10, 20, 30) as the default block configuration, which has the optimal performance in terms of quality and speed in our experiments, and does not incur excessive memory overhead.

#### 4.8 Scaling to Multi-GPUs and Higher Resolution

MixCache can be compatible with the current mainstream DiT parallel methods with a minor cache selection synchronization overhead. We integrate Ulysses parallel [8] to MixCache and present the latency on Wan 14B. As in Figure 12, the parallel version of MixCache still demonstrates a consistent strong scaling with increasing GPU configurations. Besides, this performance advantage is maintained across varying resolutions, demonstrating its effectiveness on high-resolution video generation tasks.

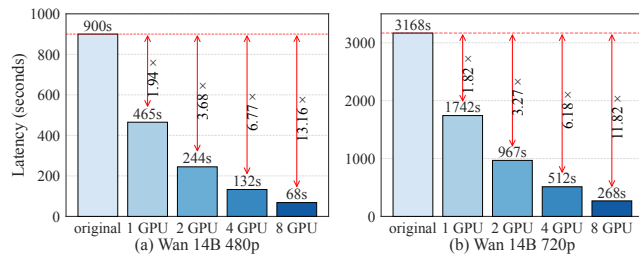


**Figure 12: Acceleration efficiency of MixCache with different video resolutions and GPU configurations.**

## 5 Conclusion

To address the high-latency challenge of video DiT inference caused by its multi-step iterative denoising process, we propose MixCache, a training-free caching-based framework for efficient video DiT inference. By leveraging the redundancy in the diffusion process of different granularities and adaptively combines three-level caching (step/cfg/block), MixCache achieves comparable generation quality while significantly improving inference efficiency, outperforming existing baselines with a maximum speedup of 1.94 $\times$  on Wan 14B and 1.97 $\times$  on HunyuanVideo. Our work establishes hybrid caching as a novel and effective approach for accelerating video DiT inference, supporting responsive multimedia content generation.

## References

- [1] Shubham Agarwal, Subrata Mitra, Sarthak Chakraborty, Srikrishna Karanam, Koyel Mukherjee, and Shiv Kumar Saini. 2024. Approximate Caching for Efficiently Serving Text-to-Image Diffusion Models. In *21st USENIX Symposium on Networked Systems Design and Implementation, NSDI 2024, Santa Clara, CA, April 15-17, 2024*, Laurent Vanbever and Irene Zhang (Eds.). USENIX Association. <https://www.usenix.org/conference/nsdi24/presentation/agarwal-shubham>
- [2] Tim Brooks, Bill Peebles, Connor Holmes, Will DePue, Yufei Guo, Li Jing, David Schnurr, Joe Taylor, Troy Luhman, Eric Luhman, et al. 2024. Video generation models as world simulators. *OpenAI Blog* 1 (2024), 8.
- [3] Pengtao Chen, Mingzhu Shen, Peng Ye, Jianjian Cao, Chongjun Tu, Christos-Savvas Bouganis, Yiren Zhao, and Tao Chen. 2024.  $\Delta$ -DiT: A Training-Free Acceleration Method Tailored for Diffusion Transformers. *CoRR* abs/2406.01125 (2024). arXiv:2406.01125 doi:10.48550/ARXIV.2406.01125
- [4] Shenggan Cheng, Yuanxin Wei, Landsong Diao, Yong Liu, Bujiao Chen, Lianghua Huang, Yu Liu, Wenyuan Yu, Jianguo Du, Wei Lin, and Yang You. 2025. SRDiffusion: Accelerate Video Diffusion Inference via Sketching-Rendering Cooperation. *CoRR* abs/2505.19151 (2025). arXiv:2505.19151 doi:10.48550/ARXIV.2505.19151
- [5] Patrick Esser, Sumith Kulal, Andreas Blattmann, Rahim Entezari, Jonas Müller, Harry Saini, Yam Levi, Dominik Lorenz, Axel Sauer, Frederic Boesel, Dustin Podell, Tim Dockhorn, Zion English, and Robin Rombach. 2024. Scaling Rectified Flow Transformers for High-Resolution Image Synthesis. In *Forty-first International Conference on Machine Learning, ICML 2024, Vienna, Austria, July 21-27, 2024*. OpenReview.net. <https://openreview.net/forum?id=FPnUhsQJ5B>
- [6] Jonathan Ho, Ajay Jain, and Pieter Abbeel. 2020. Denoising Diffusion Probabilistic Models. In *Advances in Neural Information Processing Systems 33: Annual Conference on Neural Information Processing Systems 2020, NeurIPS 2020, December 6-12, 2020, virtual*, Hugo Larochelle, Marc'Aurelio Ranzato, Raia Hadsell, Maria-Florina Balcan, and Hsuan-Tien Lin (Eds.). <https://proceedings.neurips.cc/paper/2020/hash/4c5bcfec8584af0d967f1ab10179ca4b-Abstract.html>
- [7] Ziqi Huang, Yinan He, Jiashuo Yu, Fan Zhang, Chenyang Si, Yuming Jiang, Yuanhan Zhang, Tianxing Wu, Qingyang Jin, Nattapol Chanpaisit, et al. 2024. Vbench: Comprehensive benchmark suite for video generative models. In *Proceedings of the IEEE/CVF Conference on Computer Vision and Pattern Recognition*. 21807–21818.
- [8] Sam Ade Jacobs, Masahiro Tanaka, Chengming Zhang, Minjia Zhang, Shuaiwen Leon Song, Samyam Rajbhandari, and Yuxiong He. 2023. DeepSpeed Ulysses: System Optimizations for Enabling Training of Extreme Long Sequence Transformer Models. *CoRR* abs/2309.14509 (2023). arXiv:2309.14509 doi:10.48550/ARXIV.2309.14509
- [9] Zeyinzi Jiang, Zhen Han, Chaojie Mao, Jingfeng Zhang, Yulin Pan, and Yu Liu. 2025. VACE: All-in-One Video Creation and Editing. *CoRR* abs/2503.07598 (2025). arXiv:2503.07598 doi:10.48550/ARXIV.2503.07598
- [10] Kumara Kahatapitiya, Haozhe Liu, Sen He, Ding Liu, Menglin Jia, Chenyang Zhang, Michael S. Ryoo, and Tian Xie. 2024. Adaptive Caching for Faster Video Generation with Diffusion Transformers. *CoRR* abs/2411.02397 (2024). arXiv:2411.02397 doi:10.48550/ARXIV.2411.02397
- [11] Levon Khachatryan, Andranik Movsisyan, Vahram Tadevosyan, Roberto Henschel, Zhangyang Wang, Shant Navasardyan, and Humphrey Shi. 2023. Text2Video-Zero: Text-to-Image Diffusion Models are Zero-Shot Video Generators. In *IEEE/CVF International Conference on Computer Vision, ICCV 2023, Paris, France, October 1-6, 2023*. IEEE, 15908–15918. doi:10.1109/ICCV51070.2023.01462
- [12] Weijie Kong, Qi Tian, Zijian Zhang, Rox Min, Zuozhuo Dai, Jin Zhou, Jiangfeng Xiong, Xin Li, Bo Wu, Jianwei Zhang, et al. 2024. Hunyuanvideo: A systematic framework for large video generative models. *arXiv preprint arXiv:2412.03603* (2024).
- [13] Senmao Li, Taihang Hu, Fahad Shahbaz Khan, Linxuan Li, Shiqi Yang, Yaxing Wang, Ming-Ming Cheng, and Jian Yang. 2023. Faster Diffusion: Rethinking the Role of UNet Encoder in Diffusion Models. *CoRR* abs/2312.09608 (2023). arXiv:2312.09608 doi:10.48550/ARXIV.2312.09608
- [14] Dong Liu, Jiayi Zhang, Yifan Li, Yanxuan Yu, Ben Lengerich, and Ying Nian Wu. 2025. FastCache: Cache What Matters, Skip What Doesn't. In *Proceedings of the IEEE/CVF Conference on Computer Vision and Pattern Recognition (CVPR) Workshops*.
- [15] Feng Liu, Shiwei Zhang, Xiaofeng Wang, Yujie Wei, Haonan Qiu, Yuzhong Zhao, Yingya Zhang, Qixiang Ye, and Fang Wan. 2024. Timestep Embedding Tells: It's Time to Cache for Video Diffusion Model. *CoRR* abs/2411.19108 (2024). arXiv:2411.19108 doi:10.48550/ARXIV.2411.19108
- [16] Jinming Lou, Wenyang Luo, Yufan Liu, Bing Li, Xinmiao Ding, Weiming Hu, Jiajiong Cao, Yuming Li, and Chenguang Ma. 2024. Token Caching for Diffusion Transformer Acceleration. *CoRR* abs/2409.18523 (2024). arXiv:2409.18523 doi:10.48550/ARXIV.2409.18523
- [17] Cheng Lu, Yuhao Zhou, Fan Bao, Jianfei Chen, Chongxuan Li, and Jun Zhu. 2022. DPM-Solver: A Fast ODE Solver for Diffusion Probabilistic Model Sampling in Around 10 Steps. In *Advances in Neural Information Processing Systems 35: Annual Conference on Neural Information Processing Systems 2022, NeurIPS 2022, New Orleans, LA, USA, November 28 - December 9, 2022*, Sammi Koyejo, S. Mohamed, A. Agarwal, Danielle Belgrave, K. Cho, and A. Oh (Eds.). [http://papers.nips.cc/paper\\_files/paper/2022/hash/260a14acce2a89dad36adc8eefe7c59e-Abstract-Conference.html](http://papers.nips.cc/paper_files/paper/2022/hash/260a14acce2a89dad36adc8eefe7c59e-Abstract-Conference.html)
- [18] Cheng Lu, Yuhao Zhou, Fan Bao, Jianfei Chen, Chongxuan Li, and Jun Zhu. 2022. DPM-Solver++: Fast Solver for Guided Sampling of Diffusion Probabilistic Models. *CoRR* abs/2211.01095 (2022). arXiv:2211.01095 doi:10.48550/ARXIV.2211.01095
- [19] Eric Luhman and Troy Luhman. 2021. Knowledge Distillation in Iterative Generative Models for Improved Sampling Speed. *CoRR* abs/2101.02388 (2021). arXiv:2101.02388 <https://arxiv.org/abs/2101.02388>
- [20] Zhengyao Lv, Chenyang Si, Junhao Song, Zhenyu Yang, Yu Qiao, Ziwei Liu, and Kwan-Yee K. Wong. 2024. FasterCache: Training-Free Video Diffusion Model Acceleration with High Quality. *CoRR* abs/2410.19355 (2024). arXiv:2410.19355 doi:10.48550/ARXIV.2410.19355
- [21] Xinyin Ma, Gongfan Fang, Michael Bi Mi, and Xinchao Wang. 2024. Learning-to-Cache: Accelerating Diffusion Transformer via Layer Caching. In *Advances in Neural Information Processing Systems 38: Annual Conference on Neural Information Processing Systems 2024, NeurIPS 2024, Vancouver, BC, Canada, December 10 - 15, 2024*, Amir Globersons, Lester Mackey, Danielle Belgrave, Angela Fan, Ulrich Paquet, Jakub M. Tomczak, and Cheng Zhang (Eds.). [http://papers.nips.cc/paper\\_files/paper/2024/hash/f0b1515be276f6ba82b4f2b25e50bef0-Abstract-Conference.html](http://papers.nips.cc/paper_files/paper/2024/hash/f0b1515be276f6ba82b4f2b25e50bef0-Abstract-Conference.html)
- [22] Xinyin Ma, Gongfan Fang, and Xinchao Wang. 2024. DeepCache: Accelerating Diffusion Models for Free. In *IEEE/CVF Conference on Computer Vision and Pattern Recognition, CVPR 2024, Seattle, WA, USA, June 16-22, 2024*. IEEE, 15762–15772. doi:10.1109/CVPR52733.2024.01492
- [23] Zehong Ma, Longhui Wei, Feng Wang, Shiliang Zhang, and Qi Tian. 2025. MagCache: Fast Video Generation with Magnitude-Aware Cache. arXiv:2506.09045 [cs.CV] <https://arxiv.org/abs/2506.09045>
- [24] Chenlin Meng, Robin Rombach, Ruiqi Gao, Diederik P. Kingma, Stefano Ermon, Jonathan Ho, and Tim Salimans. 2023. On Distillation of Guided Diffusion Models. In *IEEE/CVF Conference on Computer Vision and Pattern Recognition, CVPR 2023, Vancouver, BC, Canada, June 17-24, 2023*. IEEE, 14297–14306. doi:10.1109/CVPR52729.2023.01374
- [25] William Peebles and Saining Xie. 2023. Scalable Diffusion Models with Transformers. In *IEEE/CVF International Conference on Computer Vision, ICCV 2023, Paris, France, October 1-6, 2023*. IEEE, 4172–4182. doi:10.1109/ICCV51070.2023.00387
- [26] Robin Rombach, Andreas Blattmann, Dominik Lorenz, Patrick Esser, and Björn Ommer. 2022. High-Resolution Image Synthesis with Latent Diffusion Models. In *IEEE/CVF Conference on Computer Vision and Pattern Recognition, CVPR 2022, New Orleans, LA, USA, June 18-24, 2022*. IEEE, 10674–10685. doi:10.1109/CVPR52688.2022.01042
- [27] Tim Salimans and Jonathan Ho. 2022. Progressive Distillation for Fast Sampling of Diffusion Models. In *The Tenth International Conference on Learning Representations, ICLR 2022, Virtual Event, April 25-29, 2022*. OpenReview.net. <https://openreview.net/forum?id=TiDIxIplzh0>
- [28] Pratheba Selvaraju, Tianyu Ding, Tianyi Chen, Ilya Zharkov, and Luming Liang. 2024. FORA: Fast-Forward Caching in Diffusion Transformer Acceleration. *CoRR* abs/2407.01425 (2024). arXiv:2407.01425 doi:10.48550/ARXIV.2407.01425
- [29] Mingzhu Shen, Pengtao Chen, Peng Ye, Guoxuan Xia, Tao Chen, Christos-Savvas Bouganis, and Yiren Zhao. 2024. MD-DiT: Step-aware Mixture-of-Depths for Efficient Diffusion Transformers. In *Adaptive Foundation Models: Evolving AI for Personalized and Efficient Learning*. <https://openreview.net/forum?id=1jWhiakK7N>
- [30] Jiaming Song, Chenlin Meng, and Stefano Ermon. 2021. Denoising Diffusion Implicit Models. In *9th International Conference on Learning Representations, ICLR 2021, Virtual Event, Austria, May 3-7, 2021*. OpenReview.net. <https://openreview.net/forum?id=St1giarCHLP>
- [31] Ashish Vaswani, Noam Shazeer, Niki Parmar, Jakob Uszkoreit, Llion Jones, Aidan N. Gomez, Lukasz Kaiser, and Illia Polosukhin. 2017. Attention is All you Need. In *Advances in Neural Information Processing Systems 30: Annual Conference on Neural Information Processing Systems 2017, December 4-9, 2017, Long Beach, CA, USA*, Isabelle Guyon, Ulrike von Luxburg, Samy Bengio, Hanna M. Wallach, Rob Fergus, S. V. N. Vishwanathan, and Roman Garnett (Eds.). 5998–6008. <https://proceedings.neurips.cc/paper/2017/hash/3f5ee243547dee91fbd053c1c4a845aa-Abstract.html>
- [32] Ang Wang, Baole Ai, Bin Wen, Chaojie Mao, Chen-Wei Xie, Di Chen, Feiwu Yu, Haiming Zhao, Jianxiao Yang, Jianyuan Zeng, et al. 2025. Wan: Open and Advanced Large-Scale Video Generative Models. *arXiv preprint arXiv:2503.20314* (2025).
- [33] Xiang Wang, Hangjie Yuan, Shiwei Zhang, Dayou Chen, Jiuniu Wang, Yingya Zhang, Yujun Shen, Deli Zhao, and Jingren Zhou. 2023. VideoComposer: Compositional Video Synthesis with Motion Controllability. In *Advances in Neural Information Processing Systems 36: Annual Conference on Neural Information Processing Systems 2023, NeurIPS 2023, New Orleans, LA, USA, December 10 - 16, 2023*, Alice Oh, Tristan Naumann, Amir Globerson, Kate Saenko, Moritz Hardt, and Sergey Levine (Eds.). [http://papers.nips.cc/paper\\_files/paper/2023/hash/180f6184a3458fa19c28c5483bc61877-Abstract-Conference.html](http://papers.nips.cc/paper_files/paper/2023/hash/180f6184a3458fa19c28c5483bc61877-Abstract-Conference.html)

- [34] Zhou Wang, Alan C Bovik, Hamid R Sheikh, and Eero P Simoncelli. 2004. Image quality assessment: from error visibility to structural similarity. *IEEE transactions on image processing* 13, 4 (2004), 600–612.
- [35] Felix Wimbauer, Bichen Wu, Edgar Schönfeld, Xiaoliang Dai, Ji Hou, Zijian He, Artsiom Sanakoyeu, Peizhao Zhang, and etc Sam S. Tsai. 2024. Cache Me if You Can: Accelerating Diffusion Models through Block Caching. In *IEEE/CVF Conference on Computer Vision and Pattern Recognition, CVPR 2024, Seattle, WA, USA, June 16-22, 2024*. IEEE, 6211–6220. doi:10.1109/CVPR52733.2024.00594
- [36] Jay Zhangjie Wu, Yixiao Ge, Xintao Wang, Stan Weixian Lei, Yuchao Gu, Yufei Shi, Wynne Hsu, Ying Shan, Xiaoju Qie, and Mike Zheng Shou. 2023. Tune-A-Video: One-Shot Tuning of Image Diffusion Models for Text-to-Video Generation. In *IEEE/CVF International Conference on Computer Vision, ICCV 2023, Paris, France, October 1-6, 2023*. IEEE, 7589–7599. doi:10.1109/ICCV51070.2023.00701
- [37] An Yang, Baosong Yang, Binyuan Hui, Bo Zheng, Bowen Yu, Chang Zhou, Chengpeng Li, Chengyuan Li, Dayiheng Liu, Fei Huang, Guanting Dong, Haoran Wei, Huan Lin, and etc Jialong Tang. 2024. Qwen2 Technical Report. *arXiv preprint arXiv:2407.10671* (2024).
- [38] Zhuoyi Yang, Jiayan Teng, Wendi Zheng, Ming Ding, Shiyu Huang, Jiazheng Xu, Yuanming Yang, Wenyi Hong, Xiaohan Zhang, Guanyu Feng, et al. 2024. Cogvideox: Text-to-video diffusion models with an expert transformer. *arXiv preprint arXiv:2408.06072* (2024).
- [39] Zichao Yu, Zhen Zou, Guojiang Shao, Chengwei Zhang, Shengze Xu, Jie Huang, Feng Zhao, Xiaodong Cun, and Wenyi Zhang. 2025. AB-Cache: Training-Free Acceleration of Diffusion Models via Adams-Bashforth Cached Feature Reuse. *CoRR abs/2504.10540* (2025). arXiv:2504.10540 doi:10.48550/ARXIV.2504.10540
- [40] Zhihang Yuan, Hanling Zhang, Lu Pu, Xuefei Ning, Linfeng Zhang, Tianchen Zhao, Shengen Yan, Guohao Dai, and Yu Wang. 2024. DiTFastAttn: Attention Compression for Diffusion Transformer Models. In *Advances in Neural Information Processing Systems 38: Annual Conference on Neural Information Processing Systems 2024, NeurIPS 2024, Vancouver, BC, Canada, December 10 - 15, 2024*. [http://papers.nips.cc/paper\\_files/paper/2024/hash/0267925e3c276e79189251585b4100bf-Abstract-Conference.html](http://papers.nips.cc/paper_files/paper/2024/hash/0267925e3c276e79189251585b4100bf-Abstract-Conference.html)
- [41] Hui Zhang, Tingwei Gao, Jie Shao, and Zuxuan Wu. 2025. BlockDance: Reuse Structurally Similar Spatio-Temporal Features to Accelerate Diffusion Transformers. *CoRR abs/2503.15927* (2025). arXiv:2503.15927 doi:10.48550/ARXIV.2503.15927
- [42] Richard Zhang, Phillip Isola, Alexei A Efros, Eli Shechtman, and Oliver Wang. 2018. The unreasonable effectiveness of deep features as a perceptual metric. In *Proceedings of the IEEE conference on computer vision and pattern recognition*. 586–595.
- [43] Xuanlei Zhao, Xiaolong Jin, Kai Wang, and Yang You. 2025. Real-Time Video Generation with Pyramid Attention Broadcast. In *The Thirteenth International Conference on Learning Representations, ICLR 2025, Singapore, April 24-28, 2025*. OpenReview.net. <https://openreview.net/forum?id=hDBrQ4DApF>
- [44] Chang Zou, Xuyang Liu, Ting Liu, Siteng Huang, and Linfeng Zhang. 2024. Accelerating Diffusion Transformers with Token-wise Feature Caching. *CoRR abs/2410.05317* (2024). arXiv:2410.05317 doi:10.48550/ARXIV.2410.05317
- [45] Chang Zou, Evelyn Zhang, Runlin Guo, Haohang Xu, Conghui He, Xuming Hu, and Linfeng Zhang. 2024. Accelerating Diffusion Transformers with Dual Feature Caching. *arXiv preprint arXiv:2412.18911* (2024).

Received 20 February 2007; revised 12 March 2009; accepted 5 June 2009